

First-principles modeling of multiferroic RMn_2O_5

Kun Cao,¹ Guang-Can Guo,¹ David Vanderbilt,² and Lixin He ^{*1}

¹Key Laboratory of Quantum Information, University of Science and Technology of China, Hefei, 230026, People's Republic of China

²Department of Physics and Astronomy, Rutgers University, Piscataway, New Jersey 08854-8019, USA
(Dated: September 14, 2021)

We investigate the phase diagrams of RMn_2O_5 via a first-principles effective-Hamiltonian method. We are able to reproduce the most important features of the complicated magnetic and ferroelectric phase transitions. The calculated polarization as a function of temperature agrees very well with experiments. The dielectric-constant step at the commensurate-to-incommensurate magnetic phase transition is well reproduced. The microscopic mechanisms for the phase transitions are discussed.

RMn_2O_5 (R=Tb, Dy, Ho, Y etc.) belong to a very special class of multiferroics, because the ferroelectricity is driven by the magnetic ordering[1, 2, 3]. These compounds therefore possess strong magnetoelectric (ME) coupling, showing remarkable new physical effects, such as the colossal magnetodielectric [4] and magneto-polarization-flop effects [5, 6, 7], etc. The strong ME coupling effects are not only interesting in the view of fundamental physics, but also they have potential important applications in future multifunctional devices.

Because of the complex magnetic interactions and the ME coupling, RMn_2O_5 compounds undergo several magnetic and associated electric phase transitions[4, 8, 9, 10] upon cooling from room temperature to near zero temperature. Generally, these compounds transform at about 40K from a paramagnetic (PM) phase to an antiferromagnetic (AFM) phase whose magnetic ordering is initially commensurate (CM) along the a axis. This phase transition is accompanied by a ferroelectriclike transition, with the appearance of a spontaneous polarizations and a divergence of the dielectric constant. When the temperature is lowered further to about 20K, the magnetic structures become incommensurate (ICM) along the a axis, and there is a drop of the electric polarization together with the appearance of a step in the dielectric constant [4, 7, 9]. The special phase transition sequence [7, 11] is very puzzling and the driving forces for the phase transitions are not understood. It is therefore very important to explore the closely related magnetic and electric phase transitions to gain a full understanding of the microscopic mechanism of the ME coupling and novel physics in these materials.

Recent neutron scattering experiments [11, 12] as well as first-principles calculations [3, 13] suggest that the strong ME coupling in RMn_2O_5 is due to the “exchange striction” effect. However, previous first-principles calculations [3, 13] were limited to zero temperature, and did not provide information about the phase transitions. The

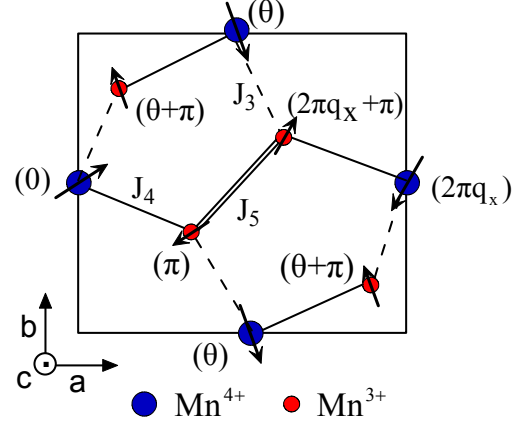


FIG. 1: (Color online) A schematic sketch of the magnetic structure projected onto the ab plane. The angle of spin orientation is given in the parentheses. The dashed, solid, and double lines represent J_3 , J_4 and J_5 exchange interactions respectively. J_1 and J_2 (not shown) are along the c -direction.

phase diagrams of RMn_2O_5 materials have been studied via a phenomenological approach [14]. This approach, based on symmetry considerations only, does not reveal any of the microscopic mechanisms of the ME coupling. In this letter, we present a first study of the phase diagrams of RMn_2O_5 materials as a function of temperature by using a first-principles effective-Hamiltonian method [15]. We obtain the most important features of the phase diagram, including the the magnetic PM-CM-ICM transitions, the accompanying ferroelectric transitions, the electric polarization as function of the temperature, and the dielectric-constant step at the CM-ICM transition.

The high-temperature crystal structure of TbMn_2O_5 is orthorhombic (space group Pbam) with four TbMn_2O_5 formula units per primitive cell, containing Mn^{4+}O_6 octahedra and Mn^{3+}O_5 pyramids [16]. The effective Hamiltonian was derived in Ref. 13 from a Heisenberg-like model. The spin-phonon coupling comes from the dependence of the exchange interactions J_α on the phonon modes u_λ . $J_\alpha(\{u_\lambda\})$ was expanded around the high-symmetry structure to second order in the phonon mode amplitudes. Five nearest-neighbor (NN) exchange inter-

*Email address: helx@ustc.edu.cn

actions were included, as sketched in Fig. 1. J_3 is the Mn^{4+} - Mn^{3+} superexchange interaction through pyramidal base corners, while J_4 is the superexchange interaction through the pyramidal apex [11]. The Mn^{3+} ions in connected pyramids couple to each other antiferromagnetically through J_5 , whereas J_1 and J_2 couple Mn^{4+} ions along the c axis.

At lower temperature a further distortion occurs, reducing the crystal symmetry to $\text{Pb2}_1\text{m}$. The lattice distortion involves 14 IR-active B_{2u} modes [3, 13]. Since the symmetry-lowering displacement is extremely small, we treated this displacement (henceforth u) as the only phonon normal mode in the model. Only the single parameter $J'_3 = \partial J_3 / \partial u$ was assumed to be involved in the first-order spin-phonon interaction. The neglect of J''_α terms, which renormalize the phonon frequencies and lead to the phonon anomalies near the magnetic phase transitions [17, 18, 19], is justified because these terms have a quite small effect on the phase diagrams studied here. The simplified Hamiltonian is then

$$E(\{u_k\}) = E_0 + \sum_k \frac{1}{2} m \omega^2 u_k^2 + \sum_{k \neq l} \frac{1}{2} \xi_{kl} u_k u_l \quad (1)$$

$$- \sum_{ij \in J_\alpha} J_\alpha(0) \mathbf{S}_i \cdot \mathbf{S}_j - \sum_{ij \in J_3} \sum_k J'_3 u_k \mathbf{S}_i \cdot \mathbf{S}_j.$$

Here E_0 is the energy of the high symmetry structure without magnetic interactions, whereas m and ω are the reduced mass and frequency of the IR-active mode, u_k is the k -th local phonon mode, and ξ_{kl} are force-constant matrix elements that couple the NN local phonon modes. This last term was absent from Ref. 13, but is included here to describe the phonon dispersion properly. We assume that the ξ_{kl} are isotropic in the ab plane, and we neglect the much smaller couplings along the c direction.

Since the RMn_2O_5 compounds have similar phase diagrams, we choose TbMn_2O_5 as an example, and determine the parameters for the simplified Hamiltonian Eq. (1) by carrying out a series of first-principles calculations on this compound [3, 13]. The calculations were based on density-functional theory within the generalized-gradient approximation (GGA) implemented in the Vienna Ab-initio Simulations Package (VASP)[20, 21]. Projector augmented-wave (PAW) pseudopotentials[22] and a 500 eV plane-wave cutoff were used. Spin polarization was included in the collinear approximation. The resulting J parameters can nevertheless be used to model noncollinear situations.

To get the spin-phonon coupling constant J'_3 , it is enough to use the energy difference ΔE between the high-symmetry and the ground-state low-symmetry structures. To simplify the notation, we redefine u to be a dimensionless parameter taking the value of unity at the ferroelectric low-symmetry state, and assign spin moments $|\mathbf{S}_i|=1.0$ as well. Then it is easy to show that $J'_3 = \Delta E/4$. We have $J'_3 \sim 1.125$ meV. In order to calcu-

late the phonon coupling constant ξ_{kl} , we calculate the total energies of different local-mode configurations. In practice, we find that including the short-range phonon interaction only has a very small effect on the results. The exchange interactions $J_1 - J_5$ were fitted to the total energies of different spin configurations and were given in Ref. 13. Alternatively, the exchange interactions can be calculated from the extended Kugel-Khomskii model [23].

In the present work, we have now also fitted the parameters to GGA+U calculations [24] with $1.0 \text{ eV} \leq U \leq 4.0 \text{ eV}$ on the Mn ions. We find that J'_3 decreases with increasing U , falling to $J'_3 = 0.325$ meV at $U = 4.0 \text{ eV}$. As we shall see, this improves the comparison of some of our later simulation results with experiment. Unfortunately, increasing U also worsens the agreement with experiment for the J parameters themselves. This tension between the fitting of J and J' parameters will be further discussed later.

We investigated the finite-temperature behavior of our effective Hamiltonian by using Monte Carlo (MC) simulations. Traditional serial-temperature MC methods have great difficulty treating systems with complex frustrated interactions. Moreover, the present system has a first-order CM-AFM-to-ICM phase transition which would be very difficult to treat using conventional methods. Here we adopt the replica-exchange method [25] in which one simulates M replicas each at a different temperature T covering a range of interest, and allows configurational exchange between the replicas. Importantly, the inclusion of high- T configurations ensures that the lower- T systems can access a broad phase space and avoid becoming trapped in local minima.

We perform the simulations on an $L \times L \times L$ cubic cell with periodic boundary conditions. Each unit cell contains eight spins and two local phonon modes. In the simulations, one MC sweep is defined to consist of a series of attempts of all variables. We performed the simulations at temperatures ranging from 3 to 90 K. The temperatures are adjusted to ensure that the exchange rates between adjacent remain close to 20%. At each T we carry out an initial 10^4 sweeps to prepare the system before allowing replica exchange. We discard these, as well as the first 10^6 sweeps after replica exchange is started, when computing equilibrium properties. Sample averages are accumulated over 2×10^6 sweeps, without replica exchange to avoid a sign problem.

We give here the results of typical simulations on a $12 \times 12 \times 12$ cell. Figures 2(a) and (b) depict the polarization and dielectric constant respectively, which are calculated via $P = \langle u \rangle$ and $\epsilon = (\langle u^2 \rangle - \langle u \rangle^2) / T$. If we use $J'_3 = 1.125$ meV and the exchange interactions are fitted from the GGA calculations, we get a single magnetic PM-to-CM-AFM transition at about 58 K, accompanied by a ferroelectric transition (shown as the dotted lines in Fig. 2). This result misses the important CM-to-ICM

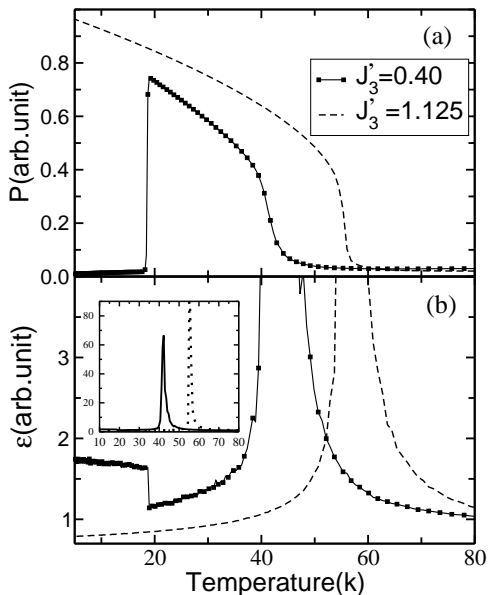


FIG. 2: (a) The electric polarization P as a function of the temperature; (b) The dielectric constant ϵ as a function of temperature for both $J_3' = 1.125$ and $J_3' = 0.4$. The inset window shows the full view of ϵ . The dielectric constants are normalized to unity at high temperature.

phase transition and overestimates the PM-to-CM transition temperature. The problem can be traced to the too-large spin-lattice coupling constant J_3' . Including the on-site Coulomb U can reduce J_3' , but at the same time it worsens the exchange interactions. We thus find that neither an effective Hamiltonian built on a pure GGA calculation, nor one built on GGA+ U with a single value of U , can give good overall agreement with experiment.

However, if we are willing to adjust the parameters by using the exchange coupling taken from pure GGA and the J_3' from GGA+ U , the situation improves dramatically. If J_3' is reduced to about 0.4 meV, as obtained from GGA+ U with $U=3$ eV, we obtain two phase transitions at about 42 and 18 K respectively, in very good agreement with experiment. The nature of each phase transition was identified via Fourier analysis of the spin configurations. At 80 K, the spins are fully disordered, indicating a PM phase. When T is lowered to 25 K, the spin spectrum shows a dominant peak at $\mathbf{q} = (0.5, 0, 0.5)$, suggesting a CM-AFM phase. The Fourier spectrum of the spin structure at 5 K shows dominant peaks at $\mathbf{q}=(5/12, 0, 0.5)$, indicating it is in the ICM phase. We therefore obtain the most important PM-CM and CM-ICM phase transitions, and the transition temperatures agree very well with the experimental values (~ 38 - 44 K for the AFM-CM ordering along the a axis, and ~ 20 K for the ICM ordering) [4, 8, 9, 10]. The calculated $q_x=5/12$ is slightly smaller than the experimental values (~ 0.46 - 0.48). It is worth noting that the calculated q_x is restricted by the supercell sizes in the simulation, which can be improved by

increasing the supercell size. Simulations on a $14 \times 14 \times 14$ cell give $q_x=3/7$. While we did not reproduce the correct q_z in both the CM and ICM phases (probably because we only have NN interactions in the model Hamiltonian), the fact that we nevertheless reproduce the correct phase transition sequence tends to confirm that the q_z value is not important for the ME coupling in these materials [3, 11].

The solid curves in Figs. 2(a) and (b) show the spontaneous polarization P and the dielectric constant ϵ as functions of T for $J_3'=0.4$ meV. The polarization increases strongly as the temperature is reduced through the PM-CM transition, but then it drops suddenly almost to zero at the CM-ICM transition. The magnetically induced polarization behaves as $P \propto \langle \mathbf{S}_3 \cdot \mathbf{S}_4 \rangle$, where \mathbf{S}_3 and \mathbf{S}_4 are the spins of the Mn^{3+} and Mn^{4+} ions coupled via the J_3 interaction. In the ICM phase, \mathbf{S}_3 and \mathbf{S}_4 are almost orthogonal (i.e., $\theta \sim \pi/2$ in Fig. 1), whereas in the CM phase they are parallel or antiparallel. These results are in excellent agreement with the experimental results for RMn_2O_5 compounds [4, 9, 11, 26], especially for YMn_2O_5 [26] and HoMn_2O_5 [9]. Note, however, that our simulation does not reproduce the reemergence of a polarized state observed experimentally in TbMn_2O_5 at still lower temperature [7]. This is probably because we ignore the spins of Tb $4f$ electrons in our model. Experimentally, it is observed that Tb is magnetically ordered below ~ 10 K, which might play an important role in the reemergence of the polarization at low T [7].

The dielectric constant shows a peak at the PM-CM transition as a consequence of the ferroelectric phase transition. Most interestingly, the dielectric constant step at the CM-ICM transition has been well reproduced in the simulation, in which ϵ jumps by about 75% in going from the CM phase at 18 K to the ICM phase. The step is very interesting and important, because it may directly relate to the colossal magnetodielectric effect, which happens just at the CM-ICM transition temperatures in these materials.

To gain a better understanding of the spin-lattice coupling effects on the magnetic and structural phase transitions, we plot the J_3' -temperature phase diagram in Fig. 3. As we see, if the spin-phonon coupling is too strong ($J_3' > 0.42$ meV), there is only a PM-CM transition, and no CM-ICM transition (as in BiMn_2O_5 [27]). In contrast, if J_3' is very small ($J_3' < 0.30$ meV), the CM state will not appear, and instead a state having spin-glass (SG) character will appear above the ICM state. The complex nature of the phase diagram is due to the frustration of the J_3 interactions. It is easy to see that the CM states do not have the lowest magnetic energies, since J_3 induces spins to rotate to decrease the energy. Since the spins have the same wave vector $q_z = 0.5$ along the c axis in both the CM and ICM phases, the interactions due to J_1 and J_2 do not change in the two phases, and can be neglected in the discussion. Accord-

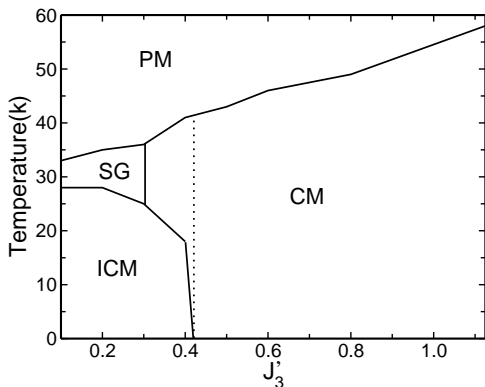


FIG. 3: The J'_3 -temperature phase diagram of the system, where PM, CM, ICM and SG represent paramagnetic, commensurate, incommensurate and spin-glass-like phase respectively.

ing to the phase factors shown in Fig. 1, the energy of the ICM state can be written as

$$E_{ICM} \approx 8J_4 - 2J_5 \cos(2\pi q_x) + 4J_3 [\cos \theta + \cos(2\pi q_x - \theta)]. \quad (2)$$

Here we assume that two spins connected by J_4 are always antiparallel to each other, because the J_4 interactions, each having two NNs, are much stronger than the J_3 and J_5 interactions. We also ignore the phonon contribution, because in the ICM phase, $\theta \sim \pi/2$ and the energy from spin-lattice coupling J'_3 is small. For the CM state, we have $\theta = 0$, $q_x = 0.5$. Therefore,

$$E_{CM} = 8J_4 + 2J_5 - 4J'_3. \quad (3)$$

The energy difference between the CM and ICM phases is determined by the competitions among J_3 , J_5 and J'_3 . In the case of $J'_3 = 1.125$ meV, the energy of the CM state is always lower than that of the ICM state, and there is no CM-ICM transition. However, when J'_3 decreases to 0.4 meV, one can find suitable θ and q_x that allow the ICM state be the ground state. Since there is no group-subgroup symmetry relation between the CM and ICM states, the phase transition between them is necessarily a first-order one. We speculate that the transition occurs because the entropy of the CM state is larger than that of the ICM state for suitable J'_3 .

The above results are calculated from the $L=12$ cell. We have also obtained similar results for the $L=10$ and 14 cells. However, due to the subtle nature of the ICM state, the parameters J_3 and J'_3 have to be slightly adjusted to produce results that are in good agreement with experiments for different cell sizes.

The “semi-empirical” philosophy we have adopted here has been to start with first-principles derived parameters, make the minimal empirical modifications to the parameters to get good agreement with experiment, and then use the resulting model to make predictions. The fact

that we have to adjust J'_3 by hand (through the choice of U) to obtain good agreement with experiment is clearly somewhat unsatisfactory. However, there is considerable precedent for such an approach. For example, in simulations of ferroelectrics via effective-Hamiltonian methods, it is a common practice to adjust the lattice constant to agree with experiment through the application of a fictitious negative pressure [15].

In summary, we have investigated the phase diagrams of RMn_2O_5 using a first-principles effective Hamiltonian method. We obtained the most important features of the phase diagrams of multiferroic RMn_2O_5 compounds, including the sequence of magnetic and ferroelectric phase transitions. Most importantly, we obtained the dielectric-constant step at the commensurate-to-incommensurate magnetic phase transition, which is key to understand the colossal magnetodielectric effects. The work further clarified the microscopic mechanism of the magnetoelectric coupling in RMn_2O_5 , and can be useful for exploring other multiferroic materials.

L.H. acknowledges the support from “Hundreds of Talents” program from CAS, and NNSF of China, Grant No. 10674124. D.V. acknowledges the support from NSF Grant DMR-0549198.

-
- [1] W. Eerenstein *et al.*, Nature **442**, 759 (2006).
 - [2] S.-W. Cheong *et al.*, Nature Materials **6**, 13 (2007).
 - [3] C. Wang *et al.*, Phys. Rev. Lett. **99**, 177202 (2007).
 - [4] N. Hur *et al.*, Phys. Rev. Lett. **93**, 107207 (2004).
 - [5] T. Kimura *et al.*, Nature **426**, 55 (2003).
 - [6] T. Goto *et al.*, Phys. Rev. Lett. **92**, 257201 (2004).
 - [7] N. Hur *et al.*, Nature **429**, 392 (2004).
 - [8] L. C. Chapon *et al.*, Phys. Rev. Lett. **96**, 097601 (2006).
 - [9] D. Higashiyama *et al.*, Phys. Rev. B **72**, 064421 (2005).
 - [10] H. Kimura *et al.*, J. Magn. Magn. Mater. **321**, 854 (2009).
 - [11] L. C. Chapon *et al.*, Phys. Rev. Lett. **93**, 177402 (2004).
 - [12] P. G. Radaelli *et al.*, Phys. Rev. B **79**, 020404(R) (2009).
 - [13] C. Wang *et al.*, Phys. Rev. B **77**, 134113 (2008).
 - [14] A. Harris *et al.*, Phys. Rev. Lett. **100**, 217202(R) (2008).
 - [15] W. Zhong *et al.*, Phys. Rev. Lett. **73**, 1861 (1994).
 - [16] J. A. Alonso *et al.*, J. Phys.: Condens. Matter **9**, 8515 (1997).
 - [17] A. F. Garcia-Flores *et al.*, Phys. Rev. B **73**, 104411 (2006).
 - [18] J. Cao *et al.*, Phys. Rev. Lett. **100**, 177205 (2008).
 - [19] T. Shen *et al.*, Phys. Rev. B **78**, 134413 (2008).
 - [20] G. Kresse *et al.*, Phys. Rev. B **47**, RC558 (1993).
 - [21] G. Kresse *et al.*, Phys. Rev. B **54**, 11169 (1996).
 - [22] P. E. Blochl, Phys. Rev. B **50**, 17953 (1994).
 - [23] H. Das *et al.*, Phys. Rev. Lett. **100**, 186402 (2008).
 - [24] G. Giovannetti *et al.*, Phys. Rev. Lett. **100**, 227603 (2008).
 - [25] R. H. Swendsen *et al.*, Phys. Rev. Lett. **57**, 2607 (1986).
 - [26] I. Kagomiya *et al.*, Ferroelectrics **286**, 167 (2003).
 - [27] A. Muñoz *et al.*, Phys. Rev. B **65**, 144423 (2002).